Supporting Information for

"Direct measurements of Fermi level pinning at the surface of intrinsically n-type InGaAs nanowires"

Maximilian Speckbacher,[†] Julian Treu,[†] Thomas J. Whittles,[‡] Wojciech M. Linhart,[‡] Xiaomo Xu,[†] Kai Saller,[†] Vinod R. Dhanak,[‡] Gerhard Abstreiter,[†] Jonathan J. Finley,[†] Tim D. Veal,*[,‡] and Gregor Koblmüller*[,†]

[†]*Walter Schottky Institut, Physik Department, and Center of Nanotechnology and Nanomaterials, Technische Universität München, Am Coulombwall 4, Garching, 85748, Germany*

[‡]*Stephenson Institute for Renewable Energy and Department of Physics, University of Liverpool, Liverpool L69 7ZF, United Kingdom*

Corresponding authors: Email: T.Veal@liverpool.ac.uk and Gregor.Koblmueller@wsi.tum.de

Additional experimental details

Excitation-power dependent photoluminescence (PL) spectroscopy

Figure S1 shows excitation-power dependent PL data of a representative as-grown InGaAs NW array (x(Ga) = 0.12), as recorded at low temperature (8K). The excitation power is varied by almost three orders of magnitude in order to reveal the two anticipated recombination mechanisms. As seen in Fig. S1(a), and in accordance with the spectra of InAs NWs of Fig. 2 in the main manuscript, the two main emission peaks E_1 and E_2 are clearly observed. While the near band edge emission appears at high transition energy of E_2 ~ 0.59 eV, the surface-mediated indirect transitions occurs red-shifted at lower energy of E_1 ~ 0.55 eV. By comparing the peak intensities of both peaks, we find that with increasing excitation power the E_2 transition rises faster than the E_1 transition. For a more quantitative analysis, we further used Gaussian peak fitting to identify the individual contributions of both these recombination mechanisms to the total PL intensity. The corresponding integrated PL intensities for the E_1 and E_2 transitions are displayed in Fig. S1(b) as a function of excitation power. We find that the PL

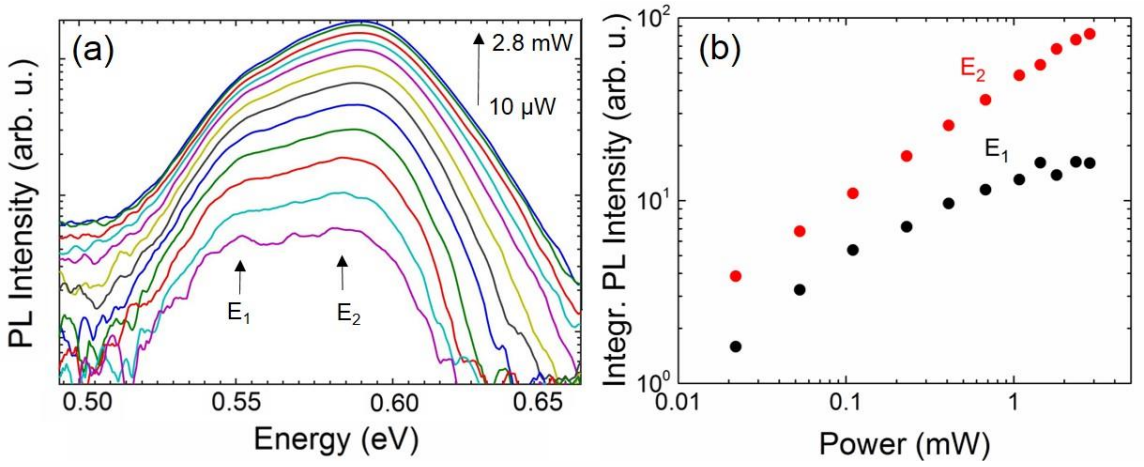

Figure S1. Excitation power dependent PL data recorded for an InGaAs NW array with x(Ga) = 0.12 at 8K; (a) measured spectra with excitation power increasing from 10 µW to 2.8 mW (bottom-to-top) in increments of ΔP~0.2-0.5 mW; (b) evolution of the integrated PL intensity as a function of excitation power for both the low-energy transition (E_1) and the high-energy transition (E_2).

intensity of the low-energy surface-mediated E_1 transition (black data points) rises only slowly (slope of $k = 0.5$) and tends to saturate at increased excitation power. In contrast, the evolution in PL intensity of the high-energy peak emission rises faster (k~0.7) with increasing excitation power (red data points), as common for the near-band edge emission of the bulk-region of InGaAs NWs.[1] The slower increase in PL intensity for the E_1 transition directly verifies the nature of the spatially indirect transitions, namely the weakened overlap of the electron and hole wave functions induced by the band bending. The fact that the E_1 transition tends to saturate towards increased excitation power can be explained by the increase in spatial separation between electrons and holes at increased carrier densities. In particular, at increased carrier densities the width of the electron accumulation layer is getting pushed closer to the surface due to the larger built-in electric fields. Hence, the spatial overlap of the surface electrons with the holes in the NW center is gradually reduced, which leads to a weakening in the quantum efficiency for this transition. Furthermore, from Fig. S1(a) we note that the peak position of the low-energy transition E_1 shifts only weakly towards the blue, i.e. ~5-10 meV closer to the E_2 peak position over the investigated excitation power range. The small sensitivity of photo-generated carrier density on the E_1 transition energy is most likely due to the fact that the intrinsic carrier densities in the electron accumulation layer are significantly in excess over the photo-generated carrier densities. Indeed, calculations of the surface charge carrier profiles (see below) reveal an average electron density of greater than 10^{18} cm^{-3} within the surface accumulation layer of an InGaAs NW with x(Ga) ~0.05.

Solutions of the Poisson equation in the modified Thomas-Fermi approximation

In order to directly estimate the surface band bending more quantitatively, we performed calculations of the surface space charge by solving the Poisson equation in the modified Thomas-Fermi approximation incorporating conduction band non-parabolicity.[2,3] In a first set

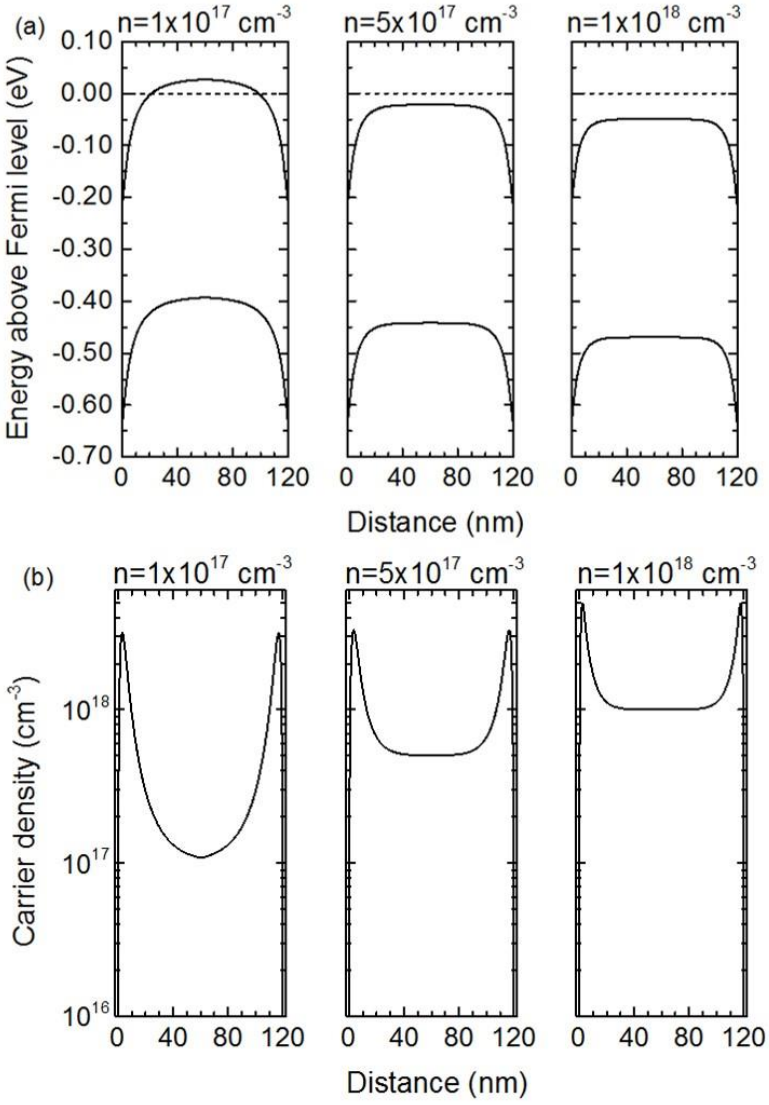

Figure S2. Band bending (a) and charge profile (b) in InGaAs NWs (x(Ga)=0.05) as a function of bulk carrier density n = 1×10^{17} cm^{-3}, 5×10^{17} cm^{-3} and 1×10^{18} cm^{-3}, as calculated by solving the Poisson equation as described in the text.

of calculations we explored the effect of carrier density on surface band bending for InGaAs NWs with x(Ga) = 0.05, in order to directly explain the excitation-power dependent evolution of the E_1 PL transition. **Figure S2** shows the calculated band bending and charge profiles of $In_{0.95}Ga_{0.05}As$ NWs, assuming a NW diameter of 120 nm in line with the experimental data. Here, the boundary conditions for the calculations were set by the VBM to Fermi level separation at the surface as determined directly from XPS, and by setting the free electron concentration to 1×10^{17} cm^{-3}, 5×10^{17} cm^{-3} and 1×10^{18} cm^{-3}. To illustrate the effect of changes to the bulk carrier density, the Fermi level was assumed to be pinned at the surface. The downward band bending is 250 meV, 200 meV and 170 meV for 1×10^{17} cm^{-3}, 5×10^{17} cm^{-3} and 1×10^{18} cm^{-3}, respectively. The width of the accumulation layer (distance from the surface to where the carrier density fall to the bulk value) decreases from 56 nm to 43 nm to 33 nm as the bulk electron concentration is changed from 1×10^{17} cm^{-3} to 5×10^{17} cm^{-3} to 1×10^{18} cm^{-3}. As a result, electrons become increasingly confined towards the surface as the carrier density increases. This effect leads to a gradual increase in the spatial separation of the electron and hole wave functions, explaining the limited quantum efficiency of the E_1 transition towards high excitation power (compare Fig. S1).

In a second set of calculations our goal is to confirm the change in downward band bending (surface electron accumulation) in In-rich InGaAs NWs to upward band bending (surface electron depletion) in more Ga-rich InGaAs NWs, in support of our composition-dependent PL experiments (Fig. 3) and XPS data (Fig. 4). **Figure S3** shows the band bending and charge profiles of InGaAs NWs with Ga-contents of x(Ga) = 0.05, x(Ga) = 0.17, and x(Ga) = 0.37 to coincide with data shown in Fig. 4. For the calculations we assumed a bulk free electron concentration of 1×10^{17} cm^{-3}, based on Seebeck effect and field effect transistor measurements of InAs NWs grown under similar conditions. Note, that the conduction band edge effective masses and dielectric constants for the wurtzite InGaAs NWs were estimated by

linear interpolation between the calculated values for wurtzite InAs and GaAs.[4,5] For x(Ga) = 0.05, the downward band bending is 250 meV, corresponding to a *donor* surface state and surface sheet electron density of 2.5×10^{12} cm^{-2} for the *accumulation* layer. For x(Ga) = 0.17, the *downward* band bending is significantly reduced to 80 meV, giving a surface sheet electron density of 4.7×10^{11} cm^{-2}. For x(Ga) = 0.37, *upward* band bending of 50 meV is present, corresponding to an *acceptor* surface state density of 2.2×10^{11} cm^{-2} and an electron *depletion* layer. These quantitative space charge calculations support the interpretations of the PL and XPS data presented in the main text.

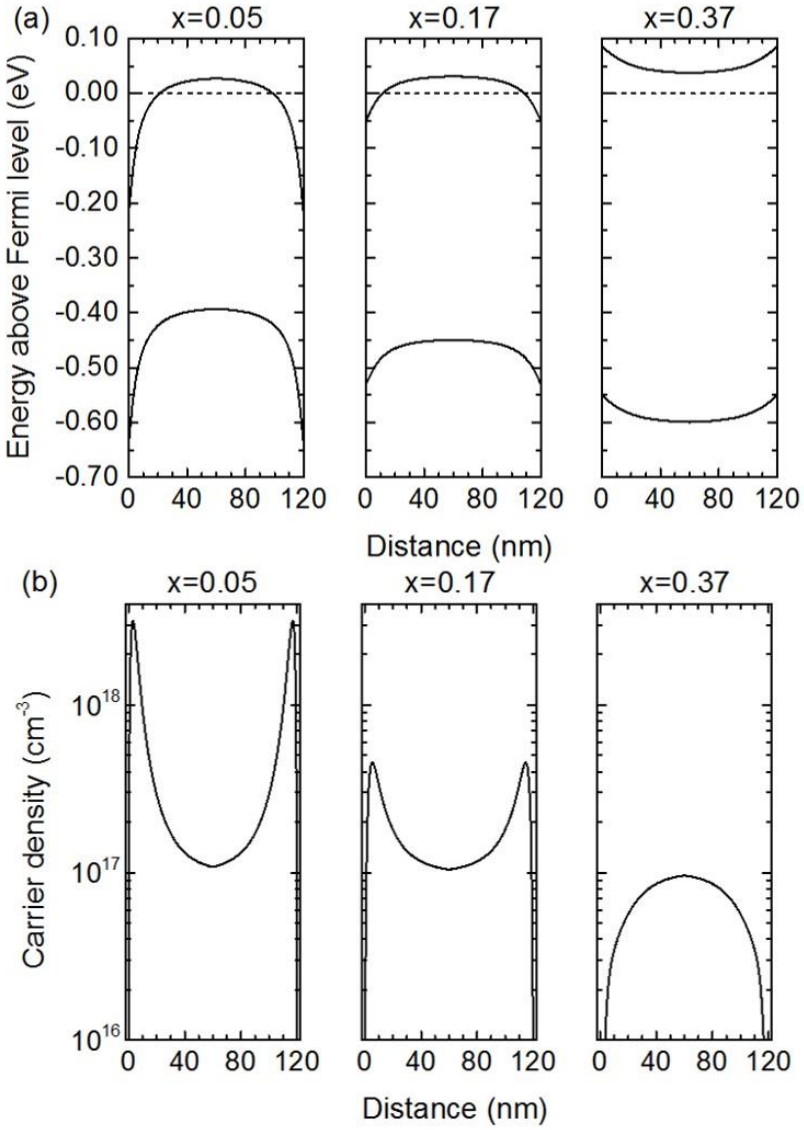

Figure S3. Band bending (a) and charge profile (b) in InGaAs NWs as a function of Ga-content x(Ga) under fixed bulk carrier density $n = 1 \times 10^{17}$ cm^{-3}.

Core-level x-ray photoemission spectroscopy (XPS) data – Nature of native oxide

Core-level XPS data was recorded at room temperature from InGaAs NW arrays containing different Ga contents of x(Ga) = 0.05, 0.17 and 0.37. The data from the InGaAs NW array with x(Ga)= 0.37 is shown and is representative of all the XPS data in so far as they all contain the same components as determined from curve fitting. The only change with increasing Ga content is that the strength of the Ga-related signals increases with respect to those related to In, as expected. Indeed, the surface Ga content from the XPS-measured In:Ga ratio is in agreement with the "bulk" composition determined from x-ray diffraction. **Figure S4** shows In 3*d* and Ga $2p_{3/2}$ XPS spectra from the InGaAs NW array with x(Ga) = 0.37. The binding energies (BEs) of the components and the full width at half maximum (FWHM) of the peaks obtained from curve fitting using CASAXPS (Ref.6) are shown in **Table S1**. All the peak assignments are consistent with previous XPS studies of InAs, GaAs and InGaAs thin films and related oxides.[7-14] The narrow, low binding energy components (solid lines) are due to In and Ga bonding to As in the NWs, shown in (a) and (b), respectively. The broader components (dashed lines) are attributed to the In-O and Ga-O bonding in the native oxide on the surface of the NWs. These components occur at higher binding energy due to the higher electronegativity of O compared to As. They are broader as a result of the greater disorder in terms of compositional and structural inhomogeneity of the native oxide when compared with the high structural quality of the NWs themselves.

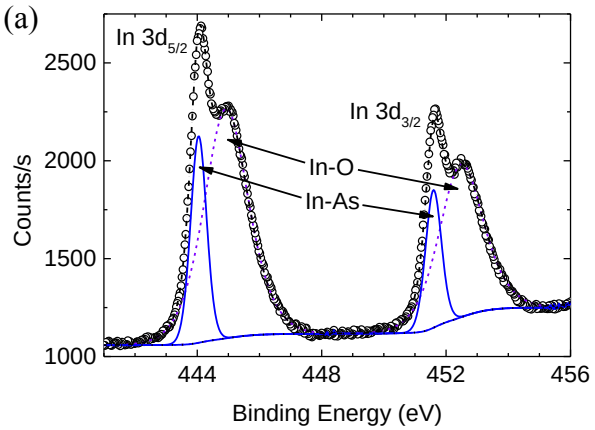

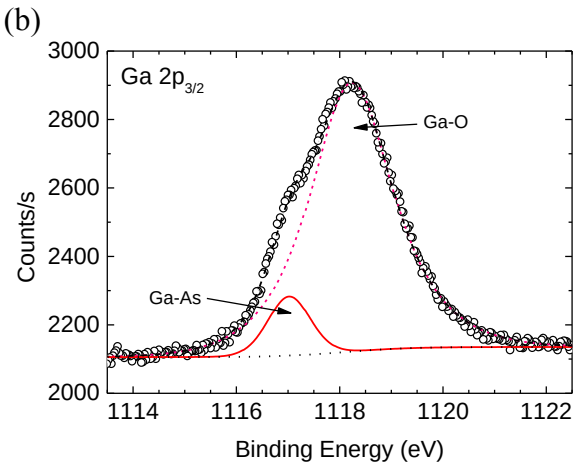

Figure S4. (a) In 3*d* photoemission spectrum from an InGaAs NW array [*x*(Ga) = 0.37] (open data points). Curve fitting resolves the spectrum into the contribution from In bonding to As (solid lines) and In bonding to oxygen (dashed lines) with the envelope total fit also shown (dash-dotted line); (b) Ga 2*p* photoemission spectrum from the same InGaAs NW array (open data points). Curve fitting resolves the spectrum into the contribution from Ga bonding to As (solid line) and Ga bonding to oxygen (dashed line) with the envelope total fit also shown (dash-dotted line).

Table S1: The binding energies (BE), with full width at half maximum (FWHM) given in parentheses, of the core level XPS peaks from the InGaAs NW array with *x*(Ga) = 0.37. The uncertainty in determining the BE of the components is typically ±0.05 eV. The separations between chemically shifted components were the same for the other two samples (*x*(Ga) = 0.05 and 0.17). Also shown is the doublet separation between the 5/2 and 3/2 peaks for the *d* levels or between the 3/2 and the 1/2 peaks for the Ga 2*p* levels that was used as a constraint in the curve fitting. The area ratios between $2p_{3/2}$ and $2p_{1/2}$ peaks and between $3d_{5/2}$ and $3d_{3/2}$ were fixed to 2:1 and 3:2, respectively.

Core Level	***In 3d5/2***	***In 4d5/2***	***Ga 2p3/2***	***Ga 3d5/2***	***As 3d5/2***
Bonding to As (eV)	444.04 (0.60)	17.34 (0.60)	1117.02 (0.97)	19.19 (0.60)	41.63 (0.76)
Bonding to O (eV)	444.93 (1.67)	18.20 (1.30)	1118.23 (1.91)	20.20 (1.30)	44.29 (1.12)
Bonding to In, Ga (eV)	-	-	-	-	40.81 (0.67)
Doublet separation (eV)	7.55	0.86	26.90	0.46	0.69

Figure S5 (a) shows the XPS spectrum from both Ga 3*d* and In 4*d* core levels from the same InGaAs NW with *x*(Ga) = 0.37. The BEs of the components and the FWHMs of the peaks obtained from curve fitting using CASAXPS [Ref.6] are shown in **Table S1**. The In 4*d* photoemission consists of two doublet peaks (blue solid curves), with each doublet being composed of $4d_{5/2}$ and $4d_{3/2}$ peaks. The narrow, lowest binding energy doublet is due to In bonding to As in the NWs and the broader, higher binding energy doublet is attributed to the In-O bonding in the native oxide on the surface of the NWs. The higher binding energy Ga 3*d* photoemission (red solid curves) has equivalent components for Ga-As and Ga-O bonding. An excellent fit is obtained to the experimental data. Although a good fit might be expected using as many as eight peaks, the fit is highly constrained by fixing the area ratios between $d_{5/2}$ and $d_{3/2}$ components at 3:2 as required by quantum mechanics, the doublet separations,[15] and by

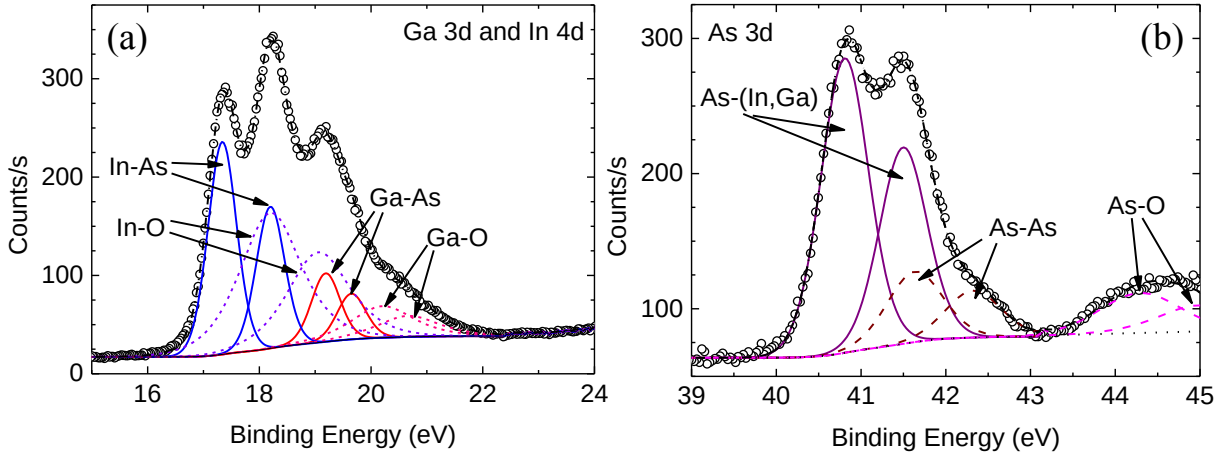

Figure S5. (a) Ga 3*d* (red lines) and In 4*d* (blue lines) photoemission spectrum from an InGaAs NW array with *x*(Ga) = 0.37 (open data points). Curve fitting resolves the spectrum into the contribution from Ga and In bonding to As (solid lines) and Ga and In bonding to oxygen (dashed lines) with the envelope total fit also shown (dash-dotted line); (b) As 3*d* photoemission spectrum from the same InGaAs NW array (open data points). Curve fitting resolves the spectrum into the contribution from As bonding to In and Ga (solid lines), that from elemental As, that is As bonding to As (dashed lines), and the component due to As bonding to oxygen. The envelope total fit is also shown (dash-dotted line).

giving equal width to both of the metal-As components and also to both of the metal-O components. Figure S5 (b) shows the XPS spectrum from the As 3*d* core level from the same InGaAs NW array. This is well fitted by three doublet components. The most intense and lowest binding energy doublet is due to the As-In and As-Ga bonding. These two contributions are indistinguishable in the As 3*d* spectrum because In and Ga have almost identical electro-negativity and so they occur at the same binding energy. The next component is due to elemental As, as previously reported for InGaAs.[14] The ratio of elemental As to III-As signal in the As 3d spectrum is about 2.5 times higher for the NW array with x(Ga) = 0.37 than for the other two investigated samples with lower Ga-content. This may be due to growth with a slightly higher V/III ratio for the highest Ga-content NW array, which is also consistent with the observation from SEM of a slightly higher density of clusters between NWs for the highest Ga content array. The highest binding energy As 3*d* component is due to As-O bonding and, as in the case of the other oxide-related XPS peaks, is broader than the NW-related peaks.

In general, the relative intensity of an oxide component is greater, the higher the binding energy of the associated core levels. This is because high binding energy corresponds to low kinetic energy and therefore lower inelastic mean free path of the photoelectrons. For example, the higher binding energy core levels such as Ga 2*p* have lower effective probing depth and so the surface native oxide contributes a greater proportion of their signal compared with lower binding energy core levels such as Ga 3*d*. For flat planar films, it is possible to use XPS to determine the thickness of the oxide by studying the attenuation of the intensity of the different binding energy InGaAs core level signals by the oxide overlayer. Such a determination is complicated in this case by the geometry of the NWs. However, it is possible to estimate that the oxide layer is less than 4 nm-thick as a contribution from the underlying InGaAs is seen in the Ga 2*p* spectrum – as the inelastic mean free path, λ, of the Ga 2*p* photoelectrons in the native indium gallium oxide is about 1.2 nm,[17] according to the Beer-Lambert law, 95% of the signal from the InGaAs would be attenuated by an overlayer of thickness 3λ = 3.6 nm.

[1] S. Morkötter, S. Funk, M. Liang, M. Döblinger, S. Hertenberger, J. Treu, D. Rudolph, A. Yadav, J. Becker, M. Bichler, G. Scarpa, P. Lugli, I. Zardo, J. J. Finley, G. Abstreiter, and G. Koblmüller, Phys. Rev. B **87**, 205303 (2013).

[2] T. D. Veal, L. F. J. Piper, W. J. Schaff, and C. F. McConville, J. Cryst. Growth **288**, 268 (2006).

[3] P. D. C. King, T. D. Veal, and C. F. McConville, Phys. Rev. B **77**, 125305 (2008).

[4] A. De and C. E. Pryor, Phys. Rev. B **81**, 155210 (2010).

[5] A. De and C. E. Pryor, Phys. Rev. B **85**, 125201 (2012).

[6] N. Fairley, http://www.casaxps.com/, ©Casa software Ltd., 2005.

[7] W. J. Stec, W. E. Morgan, R. G. Albridge, and J. R. Van Wazer, Inorg. Chem.**11**, 219 (1972).

[8] Y. Mizokawa, H. Iwasaki, R. Nishitani, and S. Nakamura, J. Electron Spect. Related Phenom.**14**, 129 (1978)

[9] F. J. Grunthaner, P. J. Grunthaner, R. P. Vasquez, B. F. Lewis, J. Maserjian, and A. Madhukar, J. Vac. Sci. Technol.**16**, 1443 (1979)

[10] H. Iwasaki, Y. Mizokawa, R. Nishitani, and S. Nakamura, Surf. Sci. **86**, 811 (1979)

[11] P. A. Bertrand, J. Vac. Sci. Technol.**18**, 28 (1981)

[12] J. R. Waldrop, E. A. Kraut, C. W. Farley, and R. W. Grant, J. Appl. Phys. **69**, 372 (1991)

[13] M. Procop, J. Electron Spect. Related Phenom. **59**, R1 (1992)

[14] F. S. Aguirre-Tostado, M. Milojevic, C. L. Hinkle, E. M. Vogel, R. M. Wallace, S. McDonnell and G. J. Hughes, Appl. Phys. Lett. **92**, 171906 (2008)

[15] J. F. Moulder, W. F. Stickle, P. E. Sobol, and K. D. Bomben, *Handbook of X-ray Photoelectron Spectroscopy*; 1995.

[16] Inelastic mean free path estimated using the NIST Electron Effective-Attenuation-Length Database, Version 1.3 available from http://www.nist.gov/srd/nist82.cfm by the method described in S. Tanuma, C. J. Powell, and D. R. Penn, Surf. Interface Anal. **21**, 165 (1994).